Direct 3D microscale imaging of C/C composites with computed holotomography

Olivia Coindreau, Gerard L. Vignoles, Peter Cloetens

Proc. E-MRS 2002 Spring Meeting, Symposium I :
Synchrotron Radiation and Materials Science,
E. Amenitsch, J. Baruchel, F. Boscherini, J. Goedkoop, and S. Heun eds.,
Nuclear Instruments and Methods in Physics Research B,
vol. **200**, pp. 295-302,
Elsevier Science, Amsterdam, Holland
(2003)

DIRECT 3D MICROSCALE IMAGING OF CARBON-CARBON COMPOSITES WITH COMPUTED HOLOTOMOGRAPHY

O. COINDREAU[1], G. VIGNOLES[1], P. CLOETENS[2]

[1] Laboratoire des Composites Thermostructuraux – UMR 5801 CNRS-Snecma-CEA-UB1
Université Bordeaux 1, 3 allée de la Boëtie, 33 600 Pessac, France
[2] European Synchrotron Radiation Facility, BP 220, 38 043 Grenoble, France

PAPER REFERENCE : I – XI.5

DIRECT 3D MICROSCALE IMAGING OF CARBON-CARBON COMPOSITES WITH COMPUTED HOLOTOMOGRAPHY

O. COINDREAU[1], G. VIGNOLES[1], P. CLOETENS[2]

[1] Laboratoire des Composites Thermostructuraux – UMR 5801 CNRS-Snecma-CEA-UB1
Université Bordeaux 1, 3 allée de la Boëtie, 33 600 Pessac, France
[2] European Synchrotron Radiation Facility, BP 220, 38 043 Grenoble, France

Abstract

As part of the modelling of CVI (Chemical Vapor Infiltration), one of the processing techniques of Carbon - Carbon composites, a better understanding of the relation between fiber architecture and transport properties is required. An excellent starting point for the pore-scale modeling of heat and gas transport is the acquisition of 3D images of the porous media through Computed Micro Tomography at various densification stages. Due to the low X-ray absorption rate of light materials such as carbon, a poor image contrast is obtained with absorption tomography. On the other hand, phase contrast imaging is readily feasible using the coherence properties of modern synchrotron beams. Holotomography has been performed on these materials and it provides quantitative density images where fibers and pyrocarbon matrix deposit are easily distinguishable. Such images are appropriate for the pore-scale computation of many effective transport properties.

Keywords : Tomography, C/C composites, phase contrast, holography.
PACS numbers : 81.70.Fy, 61.10.Yh, 81.05.Rm, 81.15.Gh

1. Introduction

Carbon-carbon composites are produced, among other processes, by chemical vapor infiltration (CVI) : it consists in densifying a heated fibrous preform by the cracking of a vapor precursor of the matrix material [1]. In addition to processing conditions (such as vapor precursor concentration, temperature and pressure), structural and transport properties of the

preform determine final characteristics of C/C composites and especially their density. As part of CVI modeling, the evolution of the structural and transport properties of the C/C composite during the densification is required to optimize its final porosity and homogeneity [2]. X-ray tomography appears as an ideal technique for nondestructive characterization at the different pore scales of 3D microstructure. Absorption tomography has already been used successfully to characterize the structure of SiC fiber cloth layup preforms at macro-porosity scale (pixel size of 15.6 μm) [3,4]. In this method, the image contrast results from the difference between the X-ray attenuation coefficient of the phases (porosity, fiber and deposit). For C/C composites, however, the difference between these coefficients is small and the contrast is faint. Therefore, we have used a new imaging method called holotomography [5,6] to characterize at microporosity scale carbon-carbon composites.

2. Principle of microtomography and holotomography

The interaction of X-rays with a medium can be described by its complex refractive index $n=1-\delta+i\beta$ [7]. The form of a plane monochromatic wave propagating along the *Z*-axis in this material is :

$$exp[-\beta\frac{2\pi}{\lambda}z]\,exp[i(1-\delta)\frac{2\pi}{\lambda}z] \qquad (1)$$

The imaginary part β determines the attenuation of the wave and the refractive index decrement δ determines the phase variation compared to propagation in vacuum. For inhomogeneous samples the transmission function *T(x,y)* is :

$$T(x,y)=exp[-\frac{2\pi}{\lambda}\int\beta(x,y,z)dz]\,exp[i(\varphi_0-\frac{2\pi}{\lambda}\int\delta(x,y,z)dz)] \qquad (2)$$

In classical absorption tomography, the detector, set directly behind the sample, measures the attenuation, which allows to calculate the integral of β along the considered path. Repeating this measurement for a large number of angular positions of the sample permits to reconstruct the $\beta(x,y,z)$ map through the use of a tomographic reconstruction algorithm [8]. Holotomography, on the other hand, allows to reconstruct the $\delta(x,y,z)$ map thanks to the knowledge of the phase distribution for each angular setting of the sample. The phase map is extracted from a series of images (three or four) recorded at different distances from the sample taking benefit of the coherence properties of third-generation synchrotron radiation beams (holographic reconstruction). Then the δ map is reconstructed with the same algorithm as in classical tomography (tomographic reconstruction). Contrast obtained with this technique is supposed to be enhanced since the ratio δ/β is much higher than unity for hard X-rays.

3. Experimental method

Experiments have been carried out on a preform made by stacking carbon fiber satin-weave (*X*-*Y* plane) held together by needlings (*Z* direction). The volume fraction of fiber is about 27%. This preform had been densified by isothermal-isobaric CVI and its core was consequently more porous than its borders. A cylindrical specimen was extracted from this bulky preform with its axis parallel to *Z*. Pieces at three different depths were sampled from it. A sample was then cut in each piece which had been previously embedded in organic resin. The diameter of those cylindrical samples is 1.3 *mm* and their length is 3 *mm*. Their macroscopic densities are 0.77 (sample 1), 1.23 (sample 2) and 1.52 (sample 3) g/cm^3.

Holotomographic experiments were performed on the ID19 line at the European Synchrotron Radiation Facility (ESRF) in Grenoble. The synchrotron X-ray beam on this line, devoted to

high-resolution imaging, shows a high lateral coherence due to the small source size and its large distance to the experimental hutch. The beam energy was set to 15 *keV* (λ=0.8339 *Å*). The sample was positioned with a precise goniometer (fine rotation and translation) and 2D radiographs were recorded every 0.12° of rotation along the vertical axis (up to 180°). Four sets of 1500 radiographs were recorded on a 2048×2048 CCD based detector [9] with sample-detector distances of 12, 50 ,150 and 500 *mm* respectively. The effective pixel size of the high resolution detector was 0.7×0.7 μm^2 and the investigated volume of material 0.9×0.9×0.7 mm^3. The average exposure time was 1 *s* and a complete acquisition lasted about two hours.

4. Results and discussion

4.1 Quantitative density images

The holotomographic reconstruction was performed for the three samples using the first three distances. This results in the 3D distribution of the refractive index decrement δ or equivalently of the electron density for each of them. Fig 1a shows a slice of the reconstructed distribution in sample 3 and fig. 1b an extract from it. The refractive index decrement δ has a much simpler dependency on the energy and the material characteristics (essentially on the electron density) than the absorption index β. For many atomic species, a good approximation of δ is [7] :

$$\delta = K \rho \lambda^2 \tag{3}$$

ρ is in g/cm^3 and λ in *Å*. 3D reconstruction of δ allows to draw the density map provided that the approximation of K is accurate enough. For materials containing mostly carbon (fiber and deposit), K is about 1.34×10^{-6} and for materials containing carbon and hydrogen (organic

resin), K is higher, about 1.42×10^{-6} for polycarbonate. Fig. 1c shows a profile along the line segment shown in Fig. 1b. The grey level is actually proportional to the reconstructed value of $-(2\pi / \lambda)\delta$ (see equation 2). The value in the region outside the sample is taken as reference. The value of δ is 1.28×10^{-6} in the region that contains resin, 1.85×10^{-6} in deposit and 1.57×10^{-6} in fiber corresponding to densities of 1.3 ± 0.2, 2 ± 0.1 and 1.7 ± 0.15 respectively. This is in agreement with expected values [10]. The profile along a line intersecting an isolated fiber has also been performed for the three samples to compare the thickness of the carbon deposit. These profiles are shown in Fig. 2. For sample 1, the deposit around the fibers is too thin to be detected on the image. Its thickness is about 7 μm in sample 2 and 9.4 μm in sample 3.

4.2 Segmented images to compute effective properties

Images of C/C composites using phase contrast at a single propagation distance had been obtained previously [11]. In this « edge detection regime », a dark/light fringe appears at density jumps. The interior of both phases (porosity and carbon) displays an indistinguishable mean grey level, while their interface appears as a double black-white layer. An image processing procedure has been designed to assign the color of its border to the interior of each phase. However, this treatment is lengthy and results are qualitative (quantitative information on density is lost). Images obtained with holotomography are expected to be segmented more easily. An extract from the reconstructed volume of sample 1 has been taken. Fig. 3 shows the histogram of grey levels. Two grey levels are easily distinguishable and correspond to the porosity and the carbon respectively. A 3D visualization of the binary image is shown in fig. 4. Another volume has been extracted from the sample 3. Its histogram in fig. 5 shows 3 grey levels corresponding respectively to carbon deposit, carbon fiber and resin. It is not easy to

separate the two carbon phases since their mean grey levels are quite close and their distributions spread out. However the mean grey levels of all forms of carbon on one hand and resin on the other hand are different enough to enable a direct segmentation of this image. However, two problems persist for the fully automated processing of the complete reconstructed data sets :

1. the image background level is not constant, so that density measurements and segmentation can only be performed locally,
2. fibers lying in a plane perpendicular to the rotation axis are prone to yield strong artifacts after reconstruction. This is probably due to the very large optical phase introduced by the fibers when beam and fiber direction are parallel.

5. Conclusions

Partially densified C/C composites have been imaged with holographic microtomography. Preliminary results validate holotomography as a quantitative tool for the determination of the density of carbon-based material parts, sensitive enough to distinguish between two types of carbon. Moreover, it provides readily segmented images of the porosity, which may then be used for the computation of effective gas transport properties [12].

6. Acknowledgments

The authors are indebted to Snecma for sample supply and thank the ESRF for providing beam time and support.

7. References

[1] R. Naslain, F. Langlais, in : J. W. Hastie, ed., *Materials Chemistry at High Temperatures*, vol. 2, Humana Press, Clifton (NJ) 1990, pp 221-235.

[2] T. L. Starr, *Mat. Res. Soc. Symp. Proc.*, vol. 250 (1992), pp. 207.

[3] J. H. Kinney, T. M. Breunig, T. L. Starr, D. Haupt, M. C. Nichols, S. R. Stock, M. D. Butts, R. A. Saroyan, *Science*, vol. 260 (1993), pp. 789-792.

[4] S-B. Lee, S. R. Stock, M. D. Butts, T. L. Starr, T. M. Breunig, J. H. Kinney, *J. Mater. Res.*, vol. 13 n°5 (1998), pp.1209-1217.

[5] P. Cloetens, W. Ludwig, J. Baruchel, D. Van Dyck, J. Van Landuyt, J. P. Guigay, M. Schlenker, *Applied Phys. Lett.* (1999), 75, pp. 2912.

[6] P. Cloetens, W. Ludwig, E. Boller, L. Helfen, L. Salvo, R. Mache, M. Schlenker, Bonse U. Ed., *Developments in X-Ray Tomography III*, vol. 4503 (2001), pp. 82-91.

[7] P. Cloetens, W. Ludwig, J. P. Guigay, J. Baruchel, M. Schlenker, D. Van Dyck, in : J. Baruchel, J.-Y. Buffiere, E. Maire, P. Merle, G. Peix, *X-ray tomography in material science*, Hermes, Paris, 2000, pp. 30-43.

[8] Robert-Coutant C., Marc A., in : J. Baruchel, J.-Y. Buffiere, E. Maire, P. Merle, G. Peix, *X-ray tomography in material science*, Hermes, Paris, 2000, pp. 61-74.

[9] J. C. Labiche, J. Segura-Puchades, D. Van Brussel, J. P. Moy, *ESRF Newsletter* n°25 (1996) , pp. 41-43.

[10] C. Sauder, *Relation microstructure / propriétés à haute température dans les fibres et matrices de carbone,* PhD Thesis, Université de Bordeaux I (in french), 2001.

[11] Vignoles G. L., *Carbon 39* (2001), pp. 167-173.

[12] O. Coindreau, G. L. Vignoles, *Etude 3D de composites C/C par microtomography X synchrotron,* Journées d'automne de la SFMM 2001 (in french).

Reference number of Manuscript : I – XI.5

List of Figure Captions

Fig. 1 : A slice (1925×1925 pix) of the reconstructed volume in sample 3 (a), an extract from it (b) and the profile along a line (c).

Fig. 2 : Profiles along 3 lines intesecting isolated fibers in sample 1, 2 and 3 respectively.

Fig. 3 : Histogram of a volume (160×200×154 voxels) extracted from sample 1.

Fig. 4 : 3D rendering of a volume extracted from sample 1.

Fig. 5 : Histogram of a volume (200×200×190 voxels) extracted from sample 3.

Reference : I-XI.5

Fig. 1

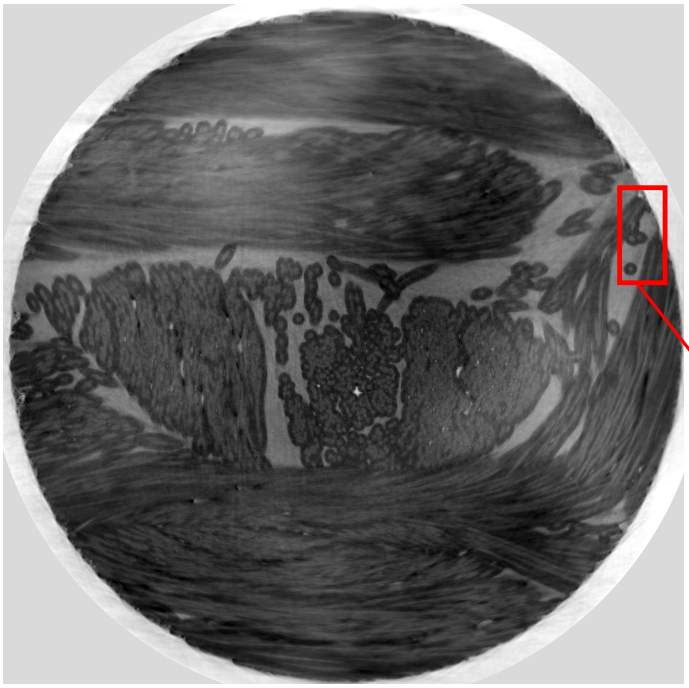

Fig. 1a

Fig. 1b

Fig. 1c

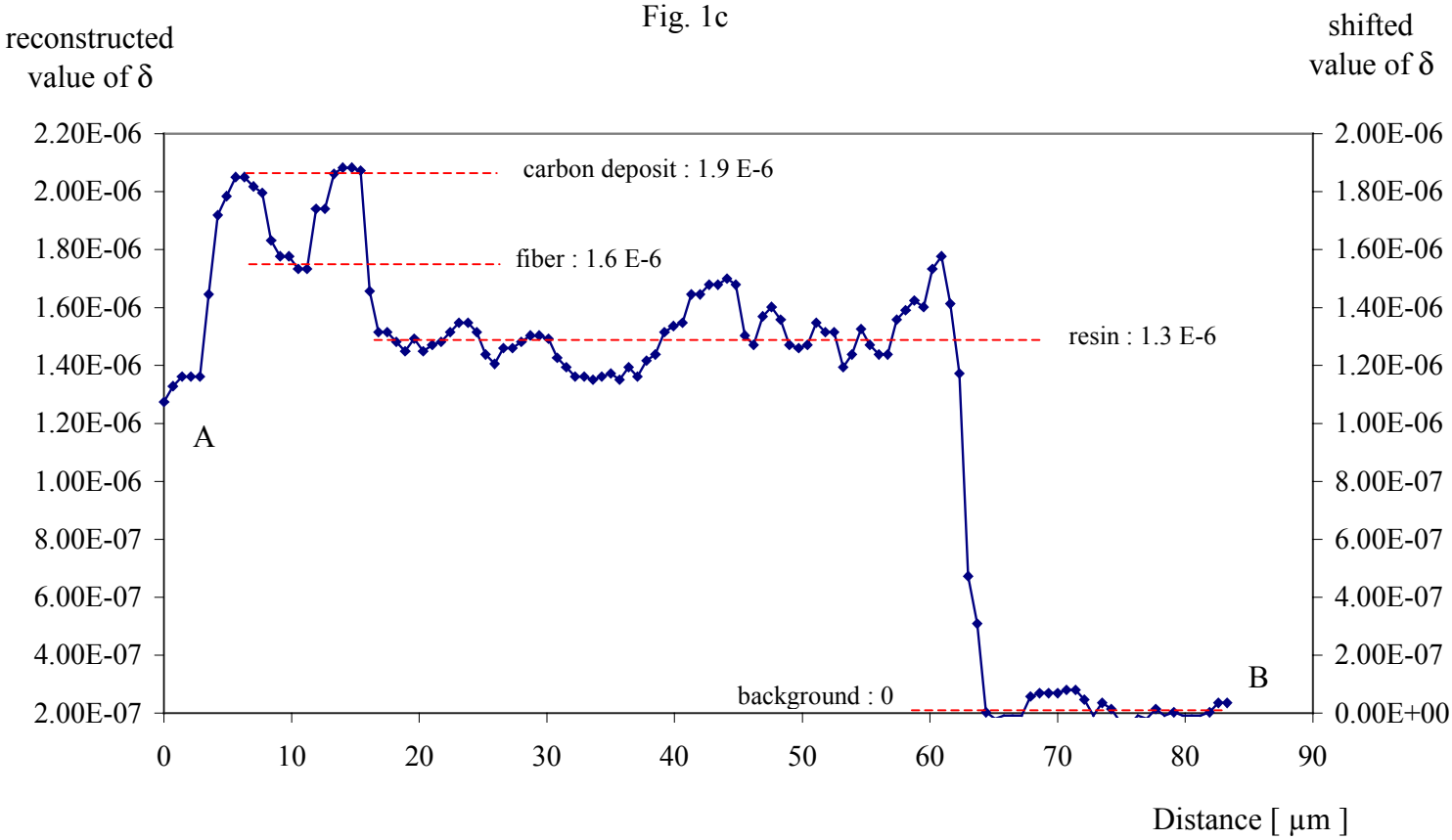

Reference : I-XI.5

Fig. 2

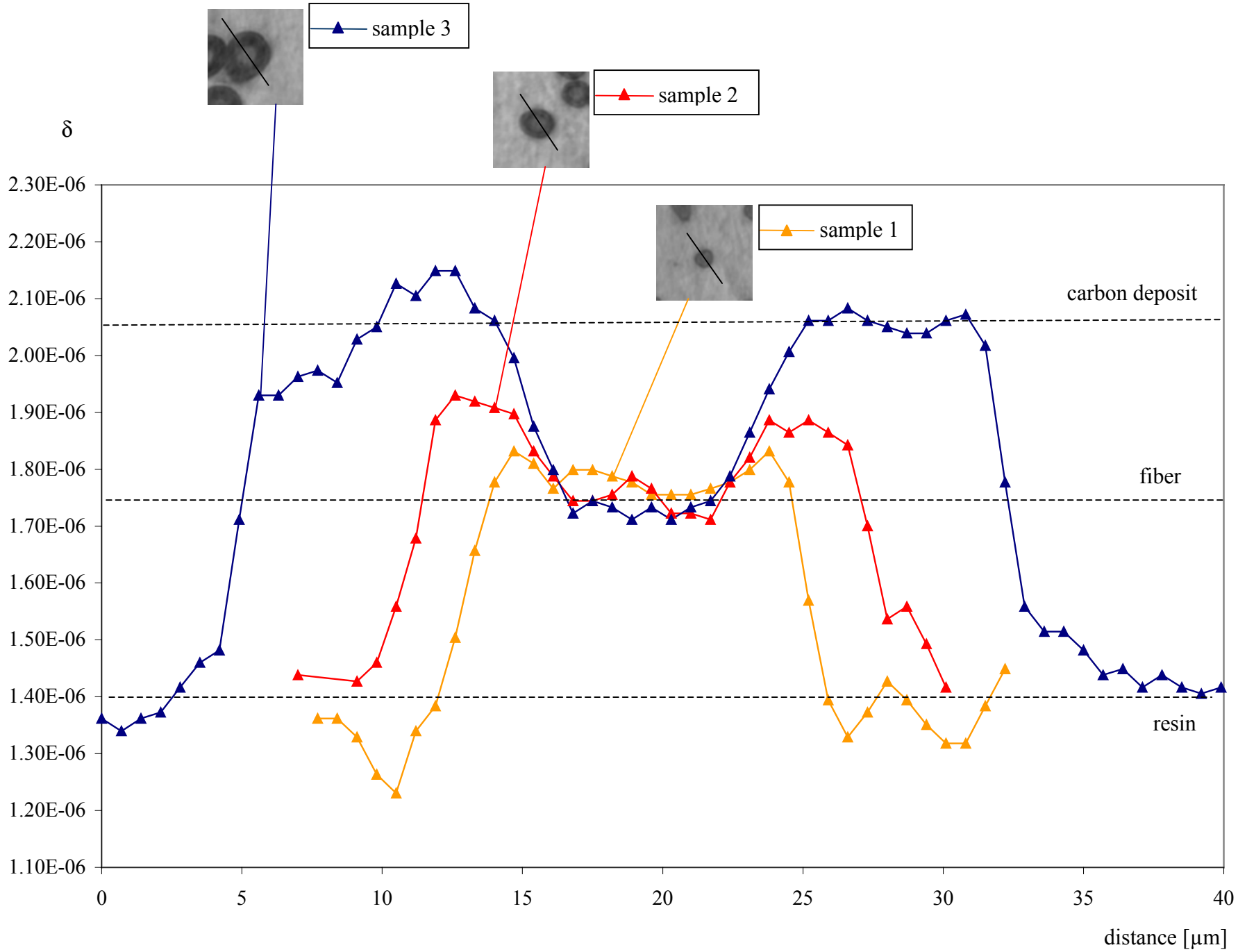

Reference : I-XI.5

Fig. 3

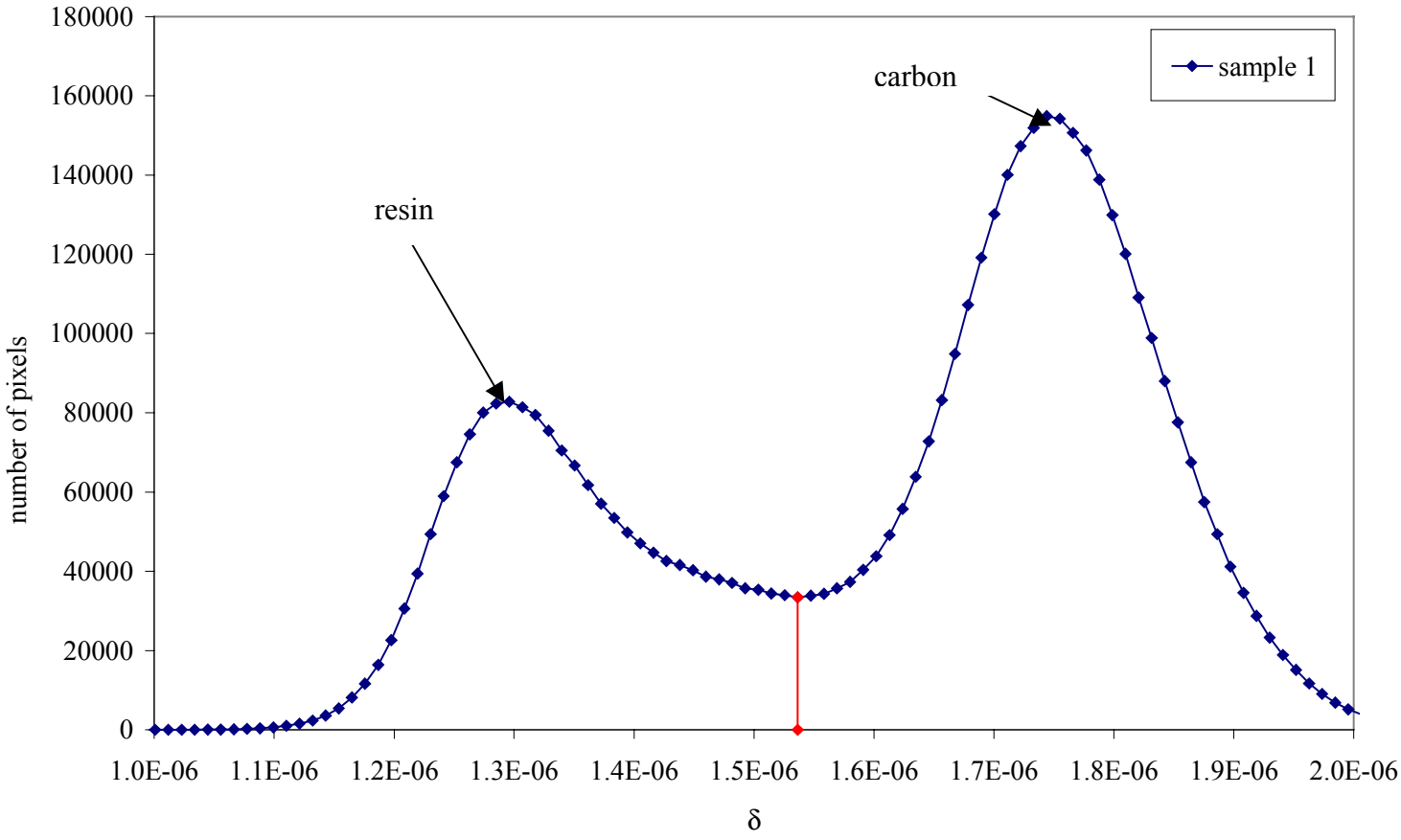

Reference : I-XI.5

Fig. 4

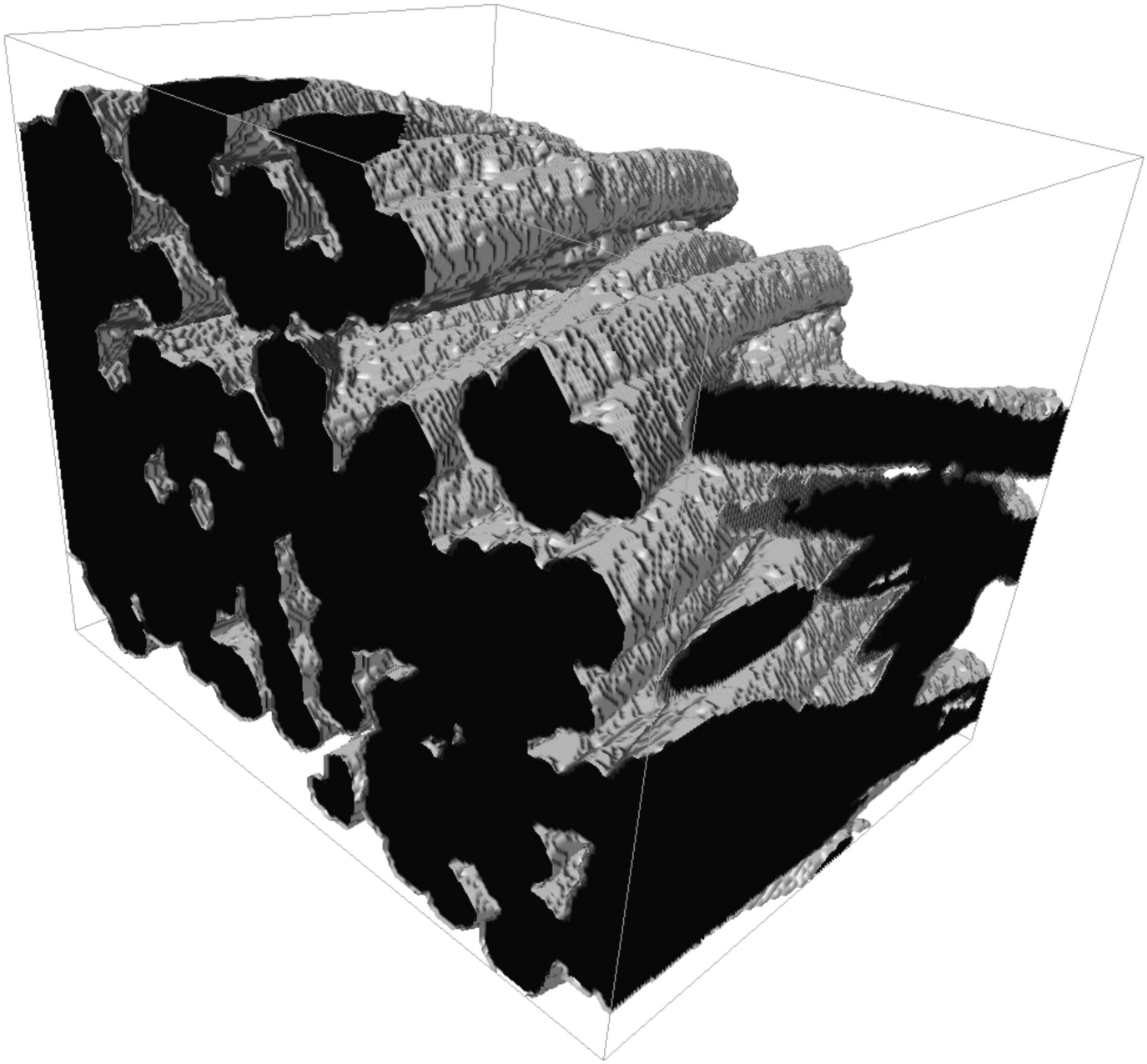

Reference : I-XI.5

Fig. 4

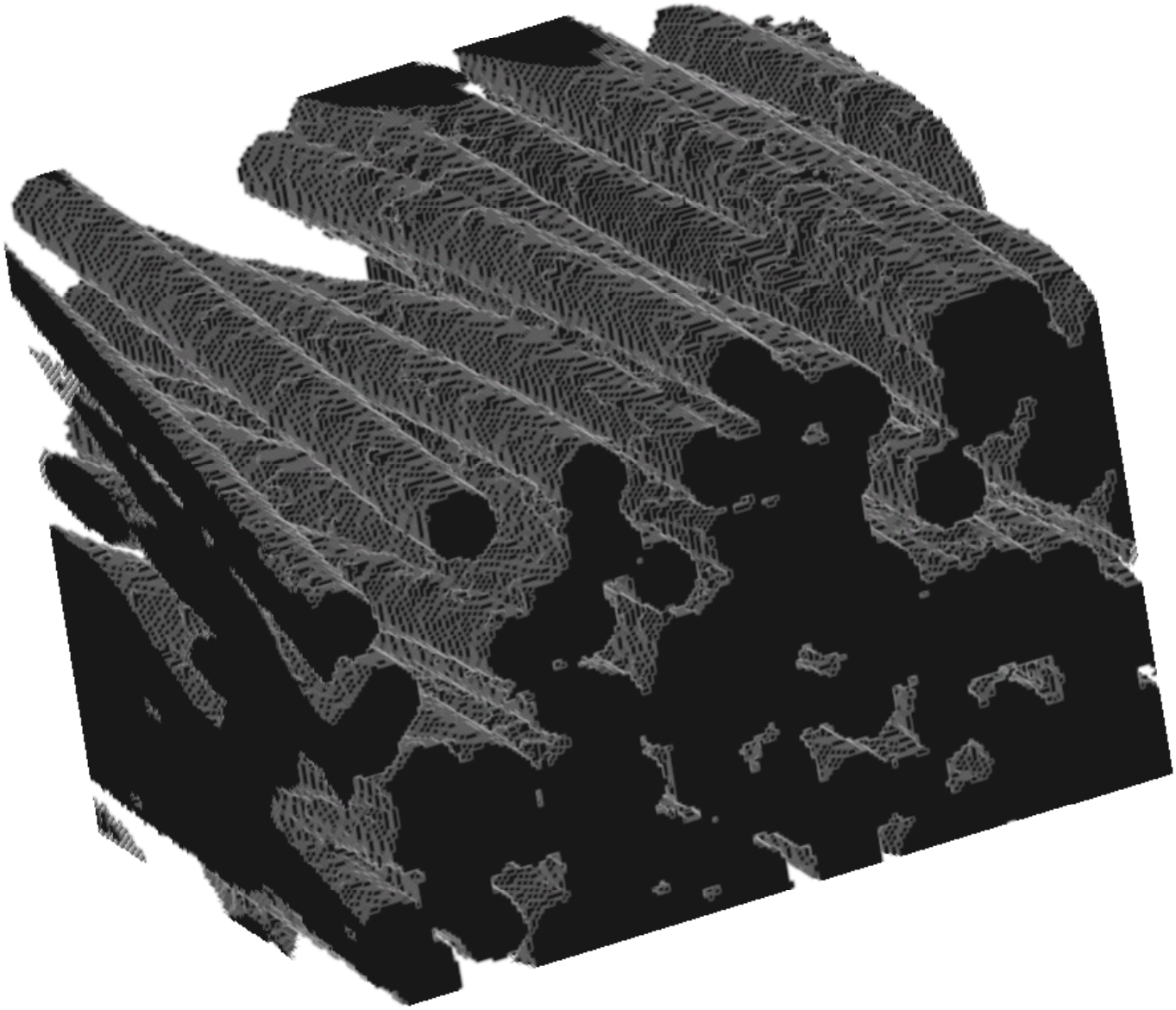

Reference : I-XI.5

Fig. 5